Journal of Chemical Health Risks

www.jchr.org

JCHR (2026) 16(2), 1292-1316 | ISSN:2251-6727

In Vitro Antioxidant and p53-Targeted Anticancer Activity of *Aerva sanguinolenta* (L.) Blume Across Different Human Cancer Cell Lines and Ehrlich Ascites Carcinoma Model

Joy Sarker [1], A.S.M. Ali Reza[2], A.B.M. Ashraful[1,3], Adeeba Anjum[1], Runa Akter[4], Md. Josim Uddin[4], Md. Sabbir Hossain[1,5], Aziz Abdur Rahman[1], Mamunur Rashid[1], Md. Golam Sadik[1], and AHM Khurshid Alam[1,4]*

[1]Department of Pharmacy, University of Rajshahi, Rajshahi-6205, Bangladesh

[2]Department of Pharmacy, International Islamic University Chittagong, Chittagong-4318, Bangladesh.

[3]Department of Pharmacy, R. P. Shaha University, Narayanganj-1400, Bangladesh.

[4]Department of Pharmacy, Independent University, Bangladesh, Dhaka-1245, Bangladesh.

[5]Department of Pharmacy, Pabna University of Science and Technology, Pabna-6600, Bangladesh.

Corresponding author

Dr. AHM Khurshid Alam, Professor, Department of Pharmacy, University of Rajshahi, Rajshahi-6205, Bangladesh.

(Received: 16 January 2026 Revised: 25 February 2026 Accepted: 17 March 2026)

KEYWORDS

Aerva sanguinolenta (L.) Blume; antioxidant; Ehrlich ascites carcinoma; HeLa cell; H-3122 cell; HEK-293 cell; ADMET.

ABSTRACT:

This study investigated the antioxidant, cytotoxic, and antitumor activities of *Aerva sanguinolenta* (L.) Blume extracts using *in vitro*, *in vivo*, and *in silico* approaches to explore its potential as a natural anticancer agent. Crude methanolic extract (CME) and its petroleum ether (PEF), chloroform (CHF), ethyl acetate (EAF), and aqueous (AQF) fractions were analyzed. Antioxidant activities were evaluated using phosphomolybdenum, ferric-reducing power, DPPH, hydroxyl radical scavenging, and lipid peroxidation assays. Cytotoxicity was assessed using MTT assays against HeLa (cervical), H-2228 and H-3122 (lung), and HEK-293 (kidney epithelial) cell lines. *In vivo* anticancer evaluation was performed in Ehrlich ascites carcinoma (EAC)–bearing mice. GC–MS identified chemical constituents, followed by p53-targeted molecular docking and ADMET predictions. CHF showed the highest phenolic and flavonoid contents, correlating with superior antioxidant activity. MTT assays revealed strong dose-dependent antiproliferative effects of CME, CHF, and EAF against HeLa cells (IC50 = 17–21 µg/mL), comparable to vincristine sulfate (VS) and 5-fluorouracil (5-FU). CHF also exhibited potent cytotoxicity against H-2228, H-3122, and HEK-293 cells, demonstrating broad-spectrum anticancer activity. In the EAC mouse model, CHF (10 mg/kg) inhibited tumor growth by 77.2%, approaching the efficacy of bleomycin. GC–MS analysis identified 17 compounds, among which 2(4H)-Benzofuranone, 5,6,7,7a-tetrahydro-4,4,7a-trimethyl-, (R)- showed the strongest p53-binding affinity. ADMET predictions indicated favorable pharmacokinetic and toxicity profiles for key candidates. *A. sanguinolenta*, particularly its chloroform fraction, shows strong antioxidant and p53-mediated anticancer potential, supporting its promise as a natural source for developing novel anticancer agents.

Introduction

Cancer continues to be one of the primary contributors to global morbidity and mortality, with GLOBOCAN 2022 estimating over 20 million new cases and nearly 9.7 million deaths annually worldwide, and incidence rates projected to escalate in the coming decades [1]. Despite notable advances in therapeutic strategies, the clinical management of cancer continues to face formidable challenges due to limited treatment efficacy, systemic toxicity, high costs, and the emergence of multidrug resistance [2]. These limitations are particularly pronounced in low and middle-income countries, underscoring the urgent need for alternative

Journal of Chemical Health Risks
www.jchr.org
JCHR (2026) 16(2), 1292-1316 | ISSN:2251-6727

and adjunctive therapeutic agents that are both efficacious and affordable [3].

A crucial pathway in the development of cancer involves oxidative stress, which occurs when the generation of reactive oxygen species (ROS) surpasses the antioxidant protective capacity [4]. Excessive ROS can induce DNA damage, lipid peroxidation, and protein oxidation, thereby activating oncogenic signaling cascades, such as PI3K/AKT, MAPK, and NF-κB pathways, while suppressing tumor suppressor pathways, including the p53 [5]. Accordingly, antioxidants capable of attenuating ROS-mediated cellular damage are increasingly recognized as potential chemopreventive and therapeutic agents [6].

Medicinal plants have long served as reservoirs of bioactive secondary metabolites, such as alkaloids, terpenoids, and polyphenols, many of which possess potent antioxidant and anticancer properties [7, 8]. Natural products remain a cornerstone of drug discovery, with over 60% of currently approved anticancer drugs being derived from or inspired by natural sources [9]. Nevertheless, numerous ethnomedicinal plants remain underexplored for their potential pharmacological benefits, including those used in traditional systems for the treatment of inflammatory and neoplastic disorders.

Aerva sanguinolenta (L.) Blume (Amaranthaceae), locally known as Lal Bish Hori, is traditionally used in Bangladesh for its sedative, diuretic, anti-inflammatory, and dermatological properties [10]. Preliminary reports have suggested antioxidant and antimicrobial effects [11], but no systematic research has investigated its phytochemical composition, antioxidant properties, or its anticancer effects across diverse cancer models. Importantly, its potential activity against human cancer cell lines, such as HeLa (cervical), H-2228 and H-3122 (lung), and HEK-293 (epithelial), remains unexplored. These cell lines are commonly used to test new anticancer agents because they have different genetic features and show different responses to antioxidant and cytotoxic compounds.

Given the traditional use of *A. sanguinolenta* and the lack of comprehensive pharmacological evaluation, we hypothesized that its phytochemical constituents may possess significant antioxidant and anticancer activities. To address this, the present study aimed to: (i) characterize the chemical profile of the crude methanolic extract and its fractions using GC–MS; (ii) evaluate antioxidant properties through multiple *in vitro* assays; (iii) assess cytotoxic activity against HeLa, H-2228, H-3122, and HEK-293 cell lines; (iv) examine *in vivo* antitumor efficacy in Ehrlich ascites carcinoma (EAC)–bearing mice; and (v) explore potential molecular targets and pharmacokinetic properties through in silico docking and ADMET analyses. This integrative approach provides the first comprehensive insight into the antioxidant and anticancer potential of *A. sanguinolenta*.

Materials and Methods

Chemicals and Reagents

All chemicals and reagents used in this study were of analytical grade and obtained from reputable suppliers. Key reagents, including Folin–Ciocalteu reagent, aluminum chloride, sodium carbonate, sodium nitrate, sodium hydroxide, hydrogen peroxide, potassium ferricyanide, ferric chloride, trichloroacetic acid, and ascorbic acid were sourced from Mark Speciality Pvt. Ltd., India, with catalogue numbers verified via Sigma-Aldrich. Methanol (MeOH) was purchased from DAEJUNG Co. Ltd., Korea. DPPH and catechin were obtained from Sigma–Aldrich, USA. Gallic acid and 2-deoxy-D-ribose were purchased from Loba Chemie, India. Sulfuric acid, EDTA, and hydrochloric acid were from Merck, Germany, while ammonium molybdate came from May & Baker, UK, and potassium ferricyanide (1%) from Meryer Chemical Technology, China.

Plant Collection

Whole plant specimens of *A. sanguinolenta* were gathered from the Rajshahi University Campus, Bangladesh (24°22'26"N 88°36'04"E) at an altitude of approximately 23 meters above sea level in November-December. The botanical identity of the collected material was then authenticated by a professional taxonomist at the Bangladesh National Herbarium, where a voucher specimen was deposited for future reference (Accession Number 46770). The collected botanical samples were cleaned under a continuous stream of pure H_2O to eliminate any dirt or debris, and then air-drying was performed at intervals with periodic sunlight exposure. Afterward, they were subjected to oven drying at a lower temperature for 24 h to achieve

Journal of Chemical Health Risks
www.jchr.org
JCHR (2026) 16(2), 1292-1316 | ISSN:2251-6727

sufficient dryness for grinding. The dried materials were then powdered via a grinder (Pharmacy Department of Rajshahi University, Bangladesh) and kept at ambient temperature until further utilization.

Extract Preparation

Approximately 500 g of dried powder was soaked in MeOH (1 L) three times and placed into a 2.5 L amber-colored extraction bottle. The powder was extracted under occasional shaking, and the solution was filtered through cotton first and then through Whatman No. 1 filter paper. The filtered extract was then concentrated via a rotary evaporator (manufactured by Yamato Scientific Co. Ltd., Chuo-ku, Tokyo, Japan) at 45 °C, yielding 80 g of crude methanolic extract (CME). From this, 35 g of CME was added to a mixture of MeOH and H_2O and subsequently fractionated first with petroleum ether, then with chloroform, and finally with ethyl acetate. This process produced four extracted samples: pet ether (PEF - 4.86 g), chloroform (CHF - 3.79 g), ethyl acetate (EAF - 9.45 g), and aqueous (AQF - 15.1 g) fractionations [12].

Gas Chromatography-Mass Spectrometry (GC–MS) Analysis of CME

GC-MS analysis was performed using a Shimadzu GC-17A system coupled with a GC–MS TQ 8040 spectrophotometer (Shimadzu Corporation, Japan), equipped with an Rxi-5 ms fused silica column (30 m × 0.32 mm, 0.25 µm film thickness). The oven was programmed from 70 °C to 220 °C with specific ramping and holding steps. Helium served as the carrier gas at a flow rate of 0.6 mL/min under a pressure of 90 kPa. The injector was set to splitless mode (3 µL), and the MS operated in EI scanning mode (40–550 m/z). Compounds were identified using the NIST library with a ≥85% match score. Quantification was based on relative peak area percentages. Data acquisition was managed using software provided by the instrument supplier [13].

Determination of Total Phenolic Content

The total phenolics were measured according to Mostofa *et al.* with slight modifications [14]. Briefly, 0.4 mL of each plant extract or standard solution was mixed with 2.0 mL of diluted Folin–Ciocalteu reagent (1:10 with deionized water) in a test tube. Subsequently, 3.0 mL of 7.5% sodium carbonate (Na_2CO_3) solution was added to each mixture. Subsequently, the absorbance of samples was measured at 765 nm after heating at 25 °C for 30 min. The total Phenolic contents were expressed as mg of Gallic acid equivalents per g of dry weight.

Determination of Total Flavonoid Content

The quantity of total flavonoids in various extracts was ascertained via the colorimetric method [15]. First, 0.5 mL of each plant extract or standard solution was placed in test tubes, followed by the addition of 150 µL of 5% $NaNO_3$ and then 2.5 mL of distilled H_2O. Five min later, 0.3 mL of 10% $AlCl_3$ was added. After 5 min, 1 mL of 4% NaOH was added, and 0.55 mL of distilled H_2O was added. The mixture was then vortexed, and the optical density was recorded at 510 nm via a photometer, with a reagent devoid of the sample serving as the reference standard. All analyses were performed in triplicate. The flavonoid content was calculated from a catechin (CA) standard curve and expressed in mg catechin equivalent per g of dry mass.

Determination of Antioxidant Capacity

Assessment of the Overall Antioxidant Capability

The phosphomolybdenum complex formation method was employed to assess the sum of the redox reduction of the different plant test samples, with some modifications [16]. A 3 mL reaction mixture comprising 0.6 M H_2SO_4, 28 mM Na_3PO_4, and 1% ammonium molybdate was poured into a test tube. Subsequently, 0.5 mL of each sample or standard was added to the mixture. The tubes were incubated at 95 °C for 10 min. Absorbance was determined at 695 nm using a UV–visible spectrophotometer after cooling to room temperature. CA was utilized as a reference standard for the evaluation.

Iron-Reducing Power Capacity

The ferric chelating power of the plant extract was assessed via the Oyaizu method [17]. A volume of 1 mL of extract at multiple concentrations was placed in test tubes. Each tube received 2.5 mL of Na_2HPO_4 buffer (0.2 M) and 2.5 mL of $K_4Fe(CN)_6$ (1%), and the mixture was subsequently incubated for 20 min at 50 °C in a water bath. After incubation, 2.5 mL of trichloroacetic acid (TCA-10%), 2.5 mL of H_2O and 0.1% $FeCl_3$ (0.5 mL) reagents were sequentially added. After the

Journal of Chemical Health Risks
www.jchr.org
JCHR (2026) 16(2), 1292-1316 | ISSN:2251-6727

reaction mixtures were subjected to centrifugal shaking, the tubes were left to stand in the dark at RT for approximately 10 min. Catechin was considered a positive control in this experiment, against which the final intensity was measured at 700 nm.

Determination of DPPH Radical Scavenging Activity

The DPPH-trapping ability of the extract was evaluated against the synthetic oxidant DPPH, as described in previous research [12, 18]. The trial was initiated by taking 1.6 mL of test samples or reference ascorbic acid (AA) into a series of test tubes, where each tube received 2.4 mL of a ready-mixed solution of 2.4 mL of DPPH and MeOH (0.1 mM). As usual, the reaction was allowed to complete by incubating the tubes under ambient conditions (25 °C) for half an hour. The transmission properties of the materials were captured via a spectrophotometer at a specific wavelength of 517 nanometers. Additionally, the same environmental conditions were maintained for the blank solution incubation. The equation mentioned below was as follows:

$$\% I = [\{A_{(control)} - A_{(sample)}\}/A_{(control)}\} \times 100$$

where $A_{control}$ is the absorbance of the DPPH solution without the sample and A_{sample} is the absorbance in the presence of the extract or standard.

Hydroxyl Radical Scavenging Activity

The hydroxyl free-radical neutralizing power of the extractives was analyzed via the known method of Halliwell *et al*. [19]. The reaction mixture contained 0.8 mL KH_2PO_4–NaOH buffer (0.05 M, pH 7.4), 2-deoxy-D-ribose (2.8 mM), 0.2 mL of test or control sample (6.25–100 µg/mL), EDTA (0.1 mM), and $FeCl_3$ (0.1 mM). Subsequently, 0.2 mL ascorbic acid (2 mM) and 0.2 mL H_2O_2 (10 mM) were added, and the mixture was incubated at 37 °C for 1 h. After incubation, 1.5 mL of 10 g/L thiobarbituric acid (TBA) in hydrochloric acid was added, boiled for 15 min, and cooled. Absorbance was measured at 532 nm against a reagent blank, and hydroxyl radical scavenging activity (%) was calculated using the equation:

$$\% \text{ Scavenging Activity} = [\{A_{(control)} - A_{(sample)}\}/A_{(control)}\} \times 100$$

where $A_{control}$ represents the absorbance of the control and A_{sample} represents the absorbance of the extracts or standard.

Lipid Peroxidation Inhibition Activity

Lipid peroxidation inhibition was assessed following a modified standard protocol [20, 21]. Bovine brain tissue was homogenized in phosphate buffer (pH 7.4) and centrifuged at 12,000 rpm for 15 min at 4 °C. The supernatant containing liposomes was collected, and 0.5 mL was mixed with 100 µL of 0.15 M KCl, 300 µL of 0.2 mM $FeCl_3$, and 100 µL of extract or standard at various concentrations to obtain a final volume of 1 mL. The mixture was incubated at 37 °C for 30 min, after which 2 mL of freshly prepared 1% TBA-TCA-BHT reagent was added and gently warmed. The mixture was subsequently incubated at 90 °C for 60 min, allowed to cool, and its absorbance was recorded at 532 nm. The percentage of lipid peroxidation inhibition was determined using the equation:

$$\% \text{ Scavenging Activity} = [\{A_{(control)} - A_{(sample)}\}/A_{(control)}\} \times 100$$

where $A_{control}$ represents the absorbance of the control and A_{sample} represents the absorbance of the extracts or standard. IC_{50} was determined from the % of inhibition versus concentration plot.

Brine Shrimp Lethality Bioassay

The Meyer method [22] was used to carry out this experiment. This study has gained popularity because it is simple, cost-effective, and quick. *Artemia salina* larvae, commonly known as brine shrimp, were hatched in filtered seawater at 25 °C for 48 h. A lamp was placed over the tank. Different plant extracts were serially diluted in DMSO and then added to 5 ml of simulated seawater containing 10 nauplii each. In the case of the control group, dimethyl sulfoxide (120 microlitres) and artificial seawater (5 mL) were used as media for the shrimp eggs, which were populated with ten nauplii each. The number of dead and surviving brine shrimp in each glass vial was counted after hatching at room temperature for one day. The LC_{50} values (50% lethal concentration in µg/mL) were determined. Vincristine sulfate (VS) at varying concentrations served as the reference drug. Mortality was assessed by comparing the

Journal of Chemical Health Risks
www.jchr.org
JCHR (2026) 16(2), 1292-1316 | ISSN:2251-6727

proportion of deaths in treated groups with that of the control group.

In Vitro Cancer Study

Cell Culture

HeLa [*Homo sapiens*; CVCL_0030; ATCC® CCL-2™], H-2228 [*Homo sapiens*; CVCL_1567; ATCC® CRL-5935™], H-3122 [*Homo sapiens*; CVCL_1904], and HEK-293 [*Homo sapiens*; CVCL_0045; ATCC® CRL-1573™] cells were purchased from the American Type Culture Collection (Manassas, VA, USA). They were maintained in a nutrient-rich solution (Dulbecco's modified Eagle's medium (DMEM)) designed to support the growth of cells *in vitro* and boosted with 10% FBS. The culture environment was maintained at 37 °C and contained 5% carbon dioxide. In all experiments, exponential-growth cells were used.

Cell Proliferation Assay

Cellular proliferation was quantified via a colorimetric assay utilizing yellow 3-(4,5-dimethythiazol- 2-yl)-2,5-diphenyl tetrazolium bromide (MTT) as described by Rahman *et al. (*2021) and Islam *et al. (*2013) [23, 24]. In brief, 5×10^3 cells were cultured in approximately 96-well plates with various concentrations of each fraction (0–500 µg/mL) for 48 h. Following treatment, 20 µL of MTT solution (5 mg/mL dissolved in PBS) was added to each well of the relevant microplate. The plate was then incubated for 4 h at 37 °C to form a purple–blue formazan precipitate. 200 µL of DMSO was mixed to dissolve the formazan crystals, resulting in a uniform purple–blue solution. The optical density (OD) was subsequently measured at 570 nm via a microplate spectrophotometer. The outcomes of the cytotoxicity assay are presented as the proportion of cytocompatibility relative to that of the control. Metrics are presented as the arithmetic mean ± standard deviation (SD). The formula used to obtain the cell viability rate was as follows:

% Viable cells = OD of samples/OD of controls × 100.

In Vivo Cancer Activity Cell Lines

Ehrlich ascites carcinoma (EAC) cells were kindly supplied by the Department of Biochemistry and Molecular Biology at the University of Rajshahi, Bangladesh. A suspension of 1×10^6 cells in 1 mL phosphate buffer was aseptically injected into the peritoneal cavity of each mouse.

Cell Growth Inhibition Assay

In vivo cytotoxicity was assessed following a previously described method [25]. For the study, the mice were organized into five groups, containing six subjects each (n = 6). Twenty-four hours after EAC cell inoculation, treatments were administered intraperitoneally for five consecutive days (1 mL/day), except for Group I. Group III and Group IV received high and low doses of *A. sanguinolenta* extract, respectively, while Group V received bleomycin. Group II, treated with saline, served as the control. On the sixth day, the mice were euthanized, and tumor cells were harvested through repeated washes with 0.9% saline. The number of viable cells was determined, and the percentage of tumor growth inhibition (%) was calculated as:

$$\% \text{ Growth inhibition} = 1 - \frac{Tw}{c_w} \times 100$$

Where T_w is the mean tumor cell count in the treatment group and C_w is the mean count in the control group. A dose–response curve was generated by plotting percentage inhibition against concentration.

In Silico Study

Protein and Ligand Preparation

For this study, the 3D crystal structure of the p53 protein (PDB ID: 1YCQ) and the selected ligands (SDF format) were retrieved from the RCSB Protein Data Bank (http://www.rcsb.org) and the PubChem database, respectively. These ligand structures were optimized through energy minimization and protonation using Avogadro software, followed by conversion to PDB format for docking studies [26]. Using BIOVIA Discovery Studio Visualizer, the α-amylase structure was refined by removing unnecessary chains, heteroatoms, and water molecules. The cleaned protein was then transformed to PDBQT format using Open Babel software.

Molecular Docking

Molecular docking was performed using AutoDock Vina integrated in PyRx to target the active site of the p53 protein with compounds identified from *A. sanguinolenta* [27]. The grid box was set to encompass the protein's substrate-binding domain, with center coordinates X = 58.6378, Y = 20.6310, Z = 34.0602 and

Journal of Chemical Health Risks
www.jchr.org
JCHR (2026) 16(2), 1292-1316 | ISSN:2251-6727

dimensions (Å) X = 40.0597, Y = 44.8869, Z = 36.0066. Docked complexes were visualized using BIOVIA Discovery Studio [26].

Pharmacokinetic Properties Analysis

SwissADME and pkCSM pharmacokinetics were employed to predict molecular properties and ADME profiles of the identified compounds [28]. The Simplified Molecular Input Line Entry System (SMILES) notation was used to generate molecular structures for analysis [29].

Toxicological Properties

Toxicity profiles of the selected compounds were evaluated using the ProTox-III web server to predict potential organ or cellular toxicity [30].

Statistical Analysis

All experiments were conducted in triplicate. The polyphenol levels and antioxidant activities are presented as mean ± standard deviation (SD), whereas the *in vivo* anticancer effects are shown as mean ± standard error of the mean (SEM). Statistical comparisons were performed through one-way ANOVA, followed by Dunnett's post hoc analysis to assess differences between treatment groups and the control. A probability value below 0.05 was considered statistically significant. Data processing and graphical representations were completed using Microsoft Excel 2016 and GraphPad Prism version 8.

Result

GC–MS Analysis

The presence of phytochemical substances in CME was investigated, and various medicinally potent chemicals were discovered, as listed in [**Table 1]** and **[Fig. 1]**. The existence of chemical components from the GC–MS spectra of the CME was validated via quantitative phytochemical screening.

Table 1: GC–MS analysis of the CME of *A. sanguinolenta.*

Name of Compounds	Chemical Class	Chemical Structure	Retention Time	*m/z*	Area	Conc.
Hexanoic acid	Fatty acid	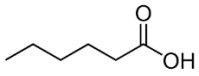	3.635	60.00	57300	1.104%
Formic acid, 2-propenyl ester	Ester	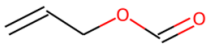	3.920	57.00	101250	1.950%
Benzeneacetaldehyde	Aromatic aldehyde	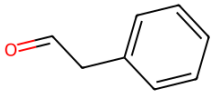	4.890	91.00	43933	0.846%
4H-Pyran-4-one, 2,3-dihydro- 3,5-dihydroxy-6-methyl-	Pyranone	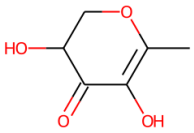	6.994	144.00	33741	0.650%

Journal of Chemical Health Risks
www.jchr.org
JCHR (2026) 16(2), 1292-1316 | ISSN:2251-6727

5-Methoxypyrrolidin-2-one	Lactam	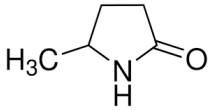	7.908	84.00	234578	4.518%
1H-Pyrrole-2,5-dione, 3-ethyl-4-methyl-	Pyrrole derivative	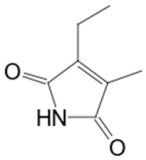	9.164	67.00	18907	0.364%
2-Methoxy-4-vinylphenol	Phenolic compound	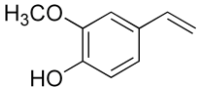	11.209	150.00	29985	0.577%
2(4H)-Benzofuranone, 5,6,7,7a-tetrahydro-4,4,7a-trimethyl-, (R)-	Benzofuran derivative	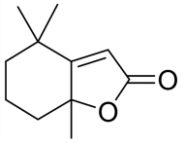	16.828	111.00	15367	0.296%
Methyl tetradecanoate	Methyl ester of fatty acid	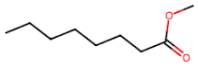	24.039	74.00	70281	1.354%
7-Hexadecenoic acid, methyl ester, (Z)-	Methyl ester of fatty acid	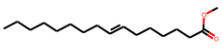	29.184	55.00	8317	0.160%
9-Hexadecenoic acid, methyl ester, (Z)-	Methyl ester of fatty acid	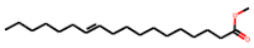	29.303	55.00	32173	0.620%
Hexadecanoic acid, methyl ester	Methyl ester of fatty acid	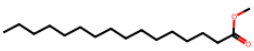	29.902	74.00	2123700	40.900%
9,12-Octadecadienoic acid, methyl ester	Methyl ester of polyunsaturated fatty acid	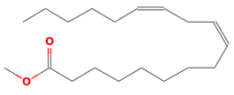	33.670	67.00	652682	12.570%
9-Octadecenoic acid, methyl ester, (E)-	Methyl ester of monounsaturated fatty acid	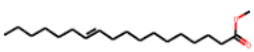	33.835	55.00	1258690	24.241%
11-Octadecenoic acid, methyl ester	Methyl ester of monounsaturated fatty acid	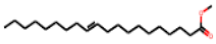	33.937	55.00	10867	0.209%

Journal of Chemical Health Risks
www.jchr.org
JCHR (2026) 16(2), 1292-1316 | ISSN:2251-6727

3,7,11,15-Tetramethyl-2-hexadecen-1-ol	Terpenoid alcohol	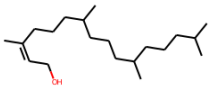	34.019	71.00	16150	0.311%
Methyl stearate	Methyl ester of saturated fatty acid	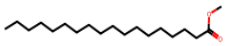	34.395	74.00	466322	8.981%

Here: Conc.: Concentration

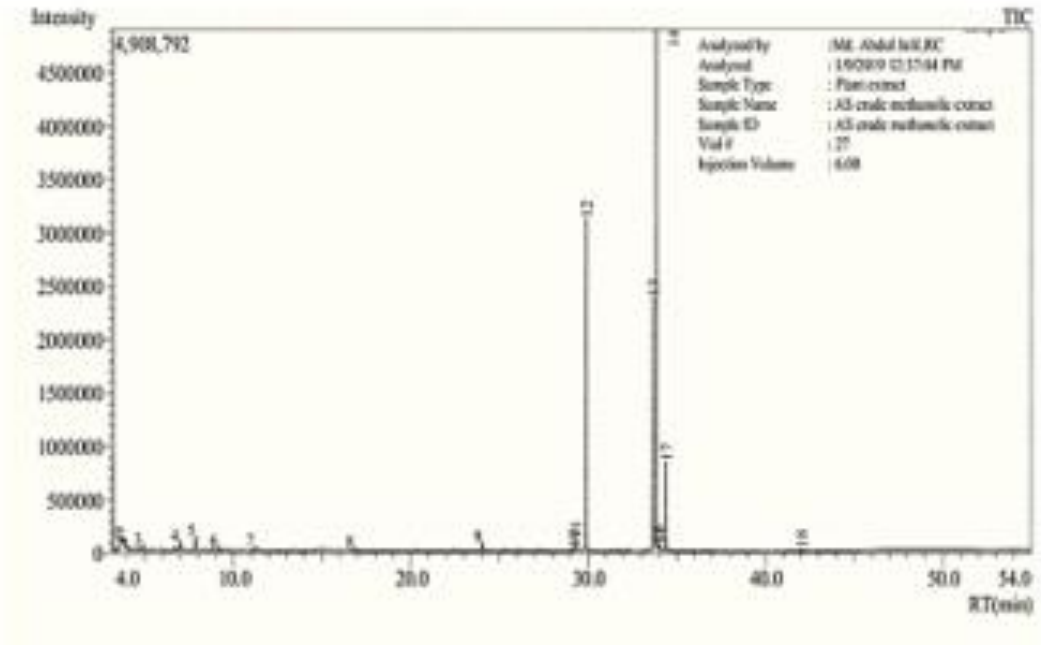

Figure 1. GC-MS spectrum of crude methanolic extract (CME) of *A. sanguinolenta*.

Determination of Total Phenolic Content

The total phenolic contents of the CME, PEF, CHF, EAF and AQF samples are shown in [**Fig. 2 (A)]**. The total phenolic content of the CHF and the EAF was greater than that of the CME. The phenolic concentrations were as follows: CHF > EAF > PEF > CME > AQF.

Determination of Total Flavonoid Content

An $AlCl_3$ chromogenic assay was performed to quantify the overall concentration of flavones in the crude methanolic mixture along with the four extracted fractions. The comprehensive flavonoid contents of the CM, PE, CH, EA and AQ fractions are shown in [**Fig. 2 (B)]**. CHF presented the maximum content of flavonoids. The order of flavonoid concentration was as follows: CHF > PEF > EAF > CME > AQF.

Evaluation of Total Antioxidant Capacity

The aggregate antioxidative capacity of the crude material and its various fractions was determined using the phosphomolybdenum technique, which involves reducing molybdenum. The comprehensive redox values of the crude drug, along with all the derivatives

Journal of Chemical Health Risks
www.jchr.org
JCHR (2026) 16(2), 1292-1316 | ISSN:2251-6727

and the reference drug (CA), are displayed in [**Fig. 2 (C)]**. Among the four derivatives, CHF exhibited the best antioxidant properties (0.932 ± 0.004), followed by PEF (0.870 ± 0.029), EAF (0.419 ± 0.001), and AQF (0.062 ± 0.009) at 100 µg/mL, whereas the intensity for catechin was 0.993 ± 0.009. These results showed that all the fractions of *A. sanguinolenta* had good antioxidative properties. The hierarchy of redox activity for various extractives and the reference CA was CA > CHF >PEF> EAF > CME > AQF.

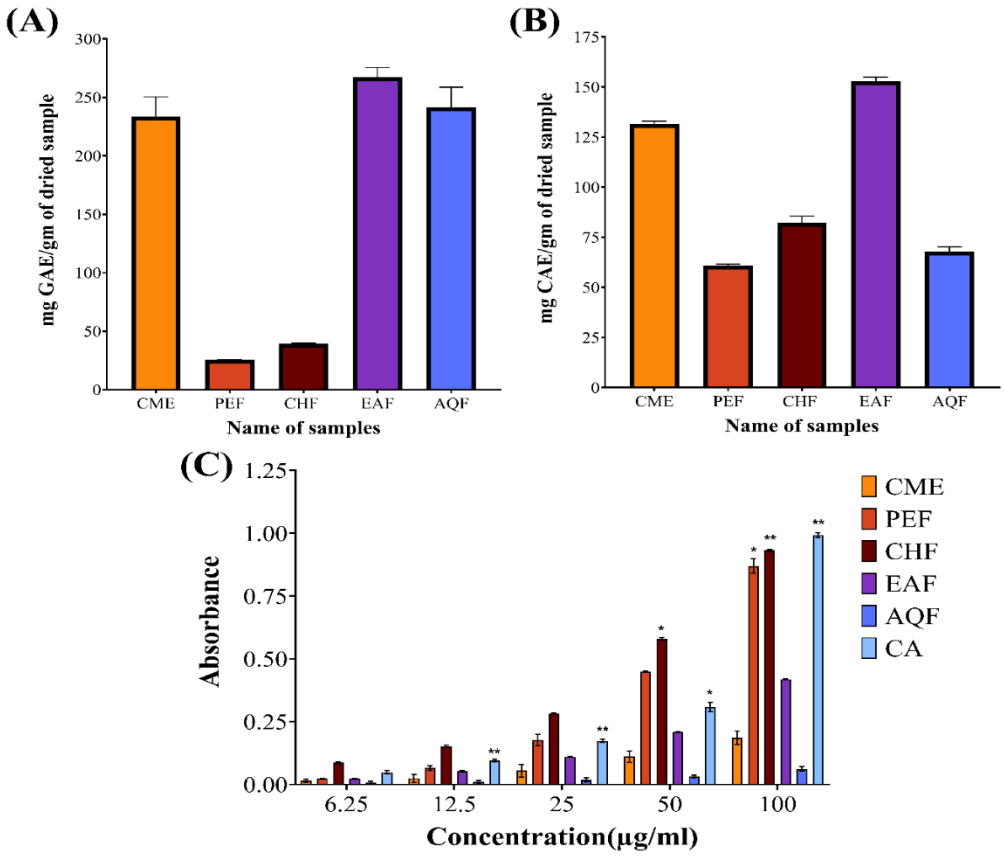

Fig. 2. (A) Determination of total phenolic content. **(B)** Determination of total flavonoid content. **(C)** Comparison of total antioxidant capacity of crude methanolic extract (CME) and its four fractions of *A. sanguinolenta* with standard catechin (CA). The data is expressed as mean ± SD (n = 3) for all tested. Values with *(*p < 0.05* and ***p < 0.01)* were considered significant.

Iron Reducing Power Capacity

The Fe^{3+} chelating power of the derivatives of *A. sanguinolenta* was evaluated via CA as a standard. The absorbance values of the extractives and reference (CA) are shown in [**Fig. 3 (A)]**. Compared with the standard CA (2.136 ± 0.005), the CHF resulted in a maximum absorbance value of 1.50 ± 0.024 among the fractions at 53.48 µg/mL. A comparison of the reducing capacity of CHF with that of the reference CA is presented in [**Fig. 3 (B)]**. The hierarchy of the reducing power capacity of the CME and its fractions was as follows: CA > CHF > EAF > CME > PEF > AQF.

Journal of Chemical Health Risks
www.jchr.org
JCHR (2026) 16(2), 1292-1316 | ISSN:2251-6727

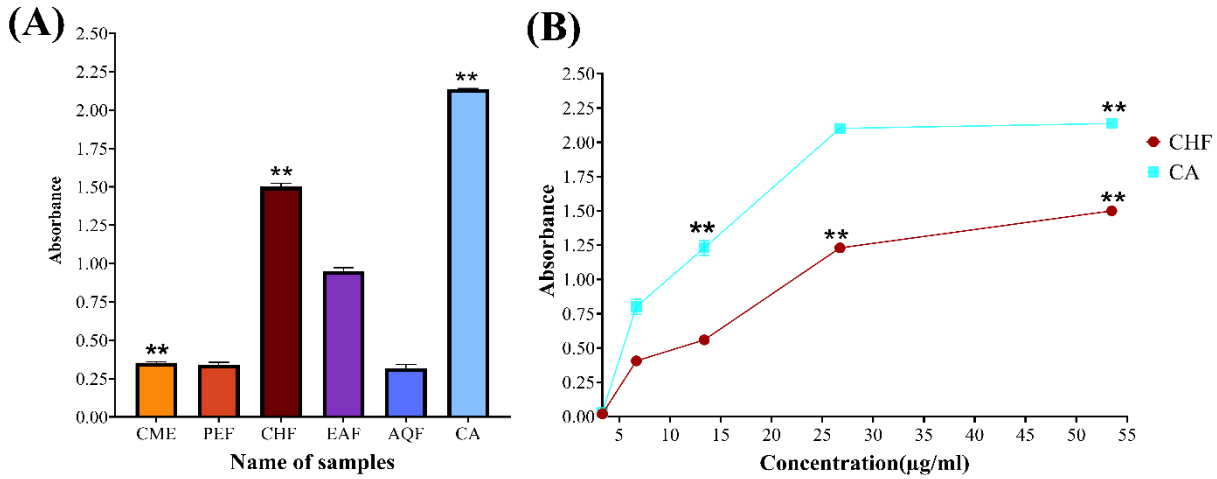

Fig. 3. (A) Determination of reducing power capacity. **(B)** Comparison of reducing power capacity of chloroform fraction (CHF) with standard catechin (CA). The data is expressed as mean ± SD (n = 3) for all tested. Values with *(*$p < 0.05$* and ***$p < 0.01$*) were considered significant.

Determination of DPPH Radical Scavenging Activity

The extractive's ability to trap persistent DPPH radicals, which possess unpaired electrons, underpins its ability to mitigate oxidative stress. The outcomes of the DPPH radical neutralization efficacy of various fractions and the standard (BHT) are presented in [**Fig. 4 (A, B)**]. The IC_{50} values of CME, PEF, CHF, EAF, AQF, and BHT were 23.98, 72.02, 11.38, 47.48, 16.63, and 7.86 µg/mL, respectively. Among the derivatives, the greatest radical neutralization activity was observed at CHF, albeit marginally inferior to that of the benchmark BHT. Conversely, PEF and EAF exhibited minimal radical neutralization efficacy. Our results demonstrated that all the extracts of *A. sanguinolenta* contained significant DPPH free radical neutralizing capabilities.

Hydroxyl Radical Scavenging Activity

The results of the analysis of the hydroxyl radical neutralization activity with the IC_{50} values of the crude CA and its different derivatives, along with those of the reference CA, are shown in [**Fig. 4 (C, D)**]. The results demonstrated that CHF, PEF, and EAF had the greatest radical neutralization efficacy, with IC_{50} values of 14, 18, and 36.05 µg/mL, respectively. The scavenging value of standard CA was 10.5 µg/mL. Therefore, our findings unequivocally revealed that the fractions of *A. sanguinolenta* possess pronounced radical-neutralizing activity. The order of hydroxyl radical scavenging ability of the different fractions and the standard CA was as follows: CA > CHF > PEF > EAF > CME > AQF.

Lipid Peroxidation Inhibition Activity

The lipid peroxidation assay outcomes of the mothers' crude samples, five fractionated samples, and CA are depicted in [**Fig. 5 (A, B)**]. Among the four fractions of CME, CHF showed the most pronounced inhibitory efficacy, with an IC_{50} value of 22.6 µg/mL, closely mirroring that of the reference CA (IC_{50} value of 17.4 µg/mL). On the other hand, PEF and EAF also had average inhibitory effects, with IC_{50} values of 32.1 and 34.3 µg/mL, respectively. The CME and AQF had lower inhibitory activities.

Brine Shrimp Lethality Bioassay

In the above bioactivity study, the CME and its four fractions showed marked biological activities. The LC_{50} values of CME and its various fractions of *A. sanguinolenta* with standard VS are displayed in [**Fig. 5 (C)**]. Vincristine sulfate was used as a positive control and had an LC_{50} value of 10.44 µg/mL. DMSO was used as a negative control and resulted in no mortality. CME had an LC_{50} of 12 µg/mL, whereas CHF had an LC_{50} value of 20 µg/mL, followed by PEF, AQF, and EAF, with LC_{50} values of 25, 25, and 38 µg/mL, respectively. The percentages of the mortality rates of the nauplii in

Journal of Chemical Health Risks
www.jchr.org
JCHR (2026) 16(2), 1292-1316 | ISSN:2251-6727

response to CME and its different fractions are shown in [**Fig. 5 (D)**].

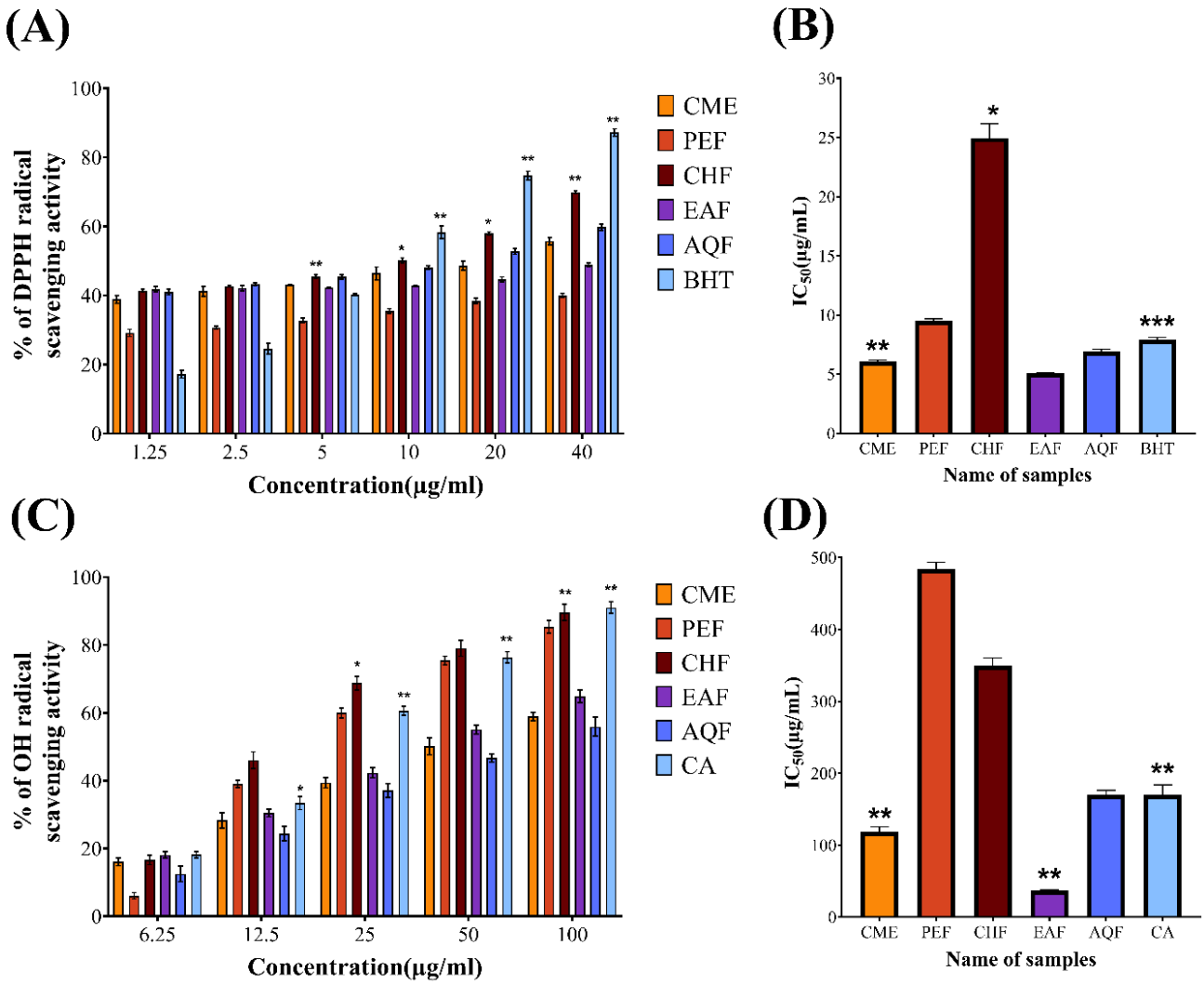

Fig. 4. (A) Determination of DPPH free radical scavenging activity. **(B)** Comparison of IC_{50} values of different extractives of *A. sanguinolenta* with standard BHT for DPPH free radical scavenging activity. **(C)** Comparison of hydroxyl radical scavenging activity. **(D)** IC_{50} (µg/mL) values of crude methanolic extract (CME) and its four fractions for hydroxyl radical scavenging with standard catechin (CA). The data is expressed as mean ± SD (n = 3) for all dosages tested. Values with *(*p < 0.05* and ***p < 0.01*) were considered significant.

Journal of Chemical Health Risks
www.jchr.org
JCHR (2026) 16(2), 1292-1316 | ISSN:2251-6727

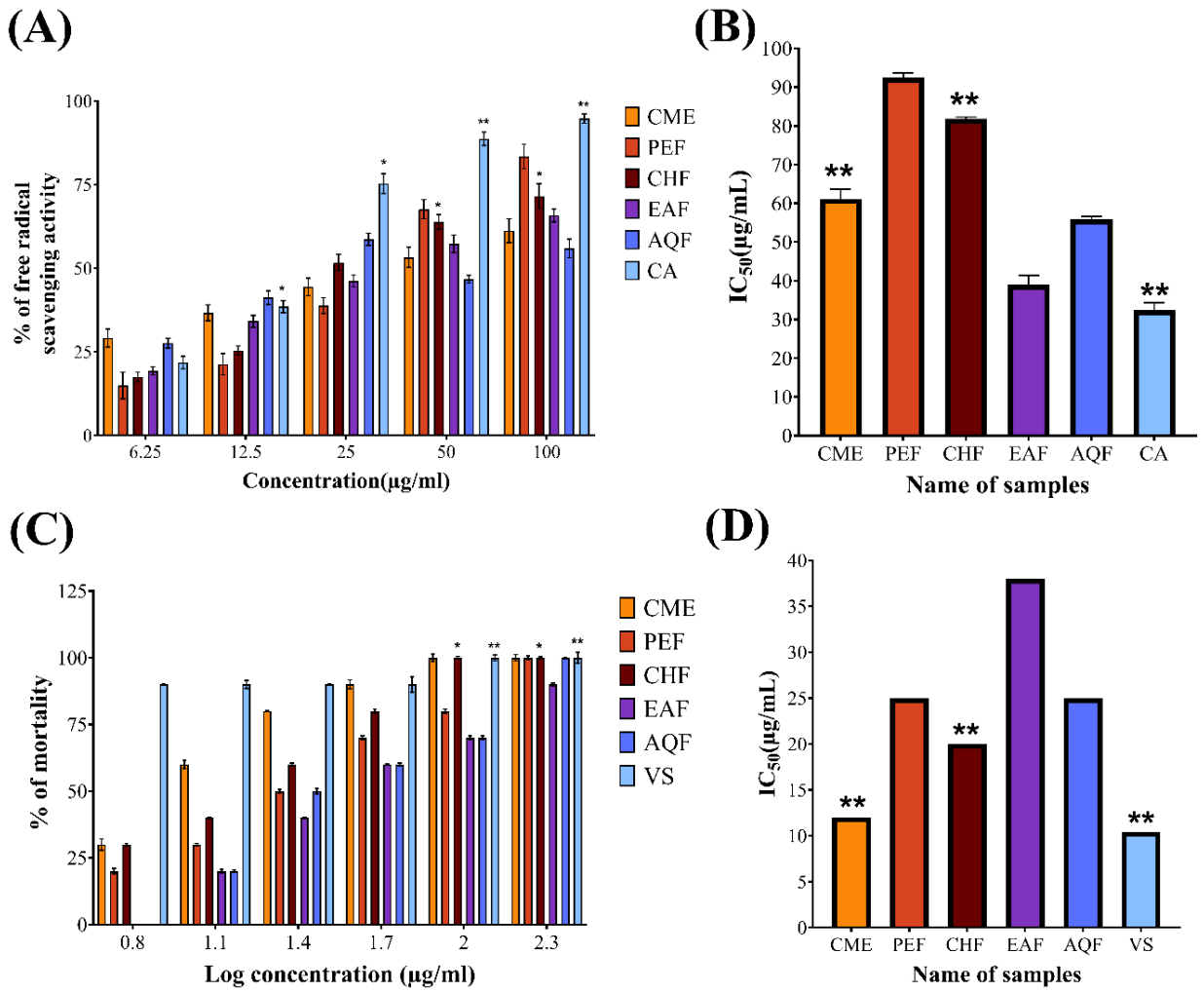

Fig. 5. (A) Comparison of lipid peroxidation inhibition activity. **(B)** IC_{50} (µg/mL) values of crude methanolic extract (CME) and its four fractions for lipid peroxidation inhibition with standard catechin (CA). **(C)** Comparative study of LC_{50} values of crude methanolic extract (CME) and its various fractions of *A. sanguinolenta* with standard vincristine sulphate (VS). **(D)** Brine shrimp lethality bioassay of crude methanolic extract (CME) and its different fractions of *A. sanguinolenta*. The data is expressed as mean ± SD (n = 3) for all dosages tested. Values with *(*$p < 0.05$* and ***$p < 0.01$*) were considered significant.

Determination of the Cytotoxic Potential of CME in the HeLa Cell Line

To determine the cytotoxicity of CME, a cellular propagation evaluation was executed via the MTT assay. HeLa cells were subjected to a range of concentrations (0–500 µg/mL) of the investigational sample, CME [**Fig. 6 (C)**]. The visual outcomes from the MTT assay wells [**Fig. 6 (A)**] and microscopic observations of treated HeLa cells [**Fig. 6 (B)**] clearly demonstrated reduced cell density and increased morphological deterioration following CME exposure.

Cytotoxicity Activity of Different Fractions of CME in the HeLa Cell Line

To assess the cytotoxicity of different fractions of CME, a cell proliferation assay was further performed

Journal of Chemical Health Risks
www.jchr.org
JCHR (2026) 16(2), 1292-1316 | ISSN:2251-6727

via MTT. Among the fractions, CHF and EAF resulted in the greatest inhibition of HeLa cell proliferation, with IC_{50} values of 20 and 21 µg/mL, respectively, which nearly resembled those of the standards VS (IC_{50} of 15 µg/mL) and 5-FU (IC_{50} of 16 µg/mL) shown in [**Fig. 6 (D)**], suggesting that CHF and EAF might have strong cytotoxic activity.

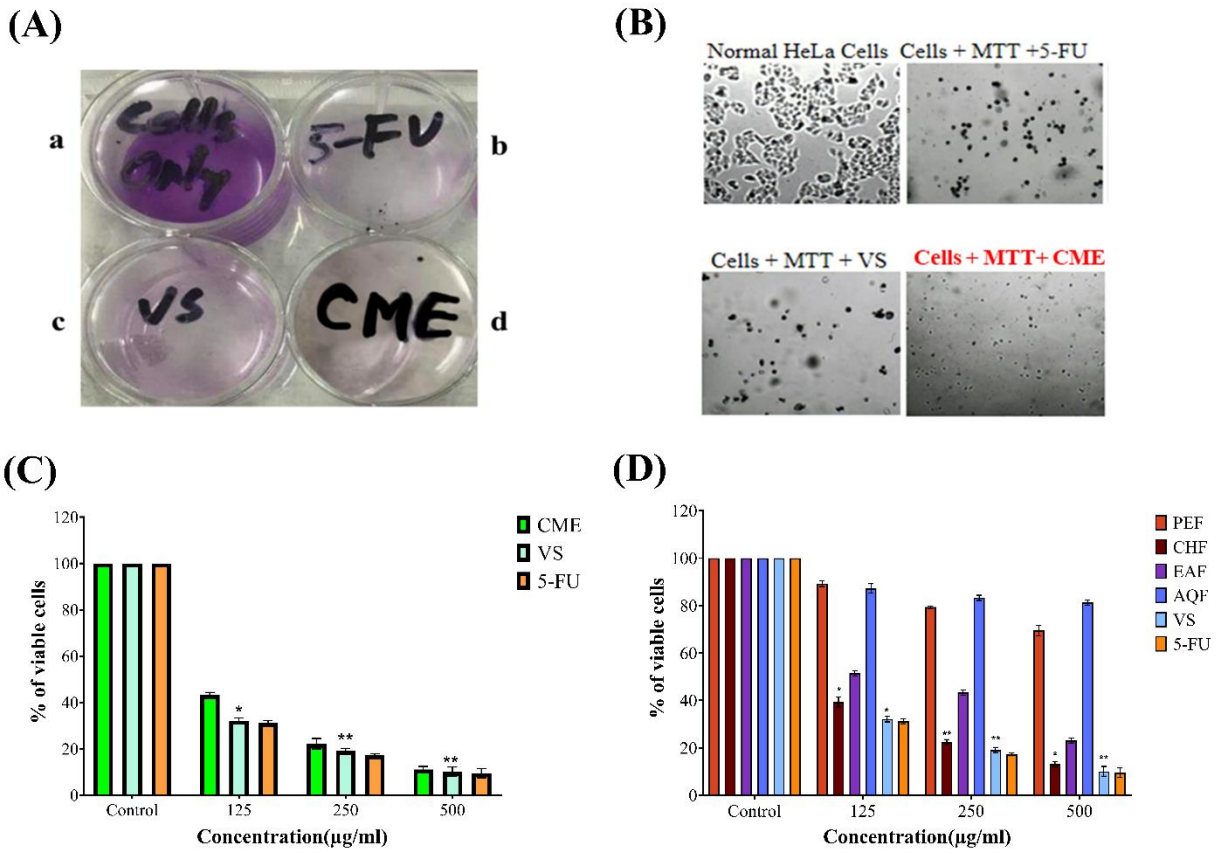

Fig. 6. (A) Visual observation, **(B)** Microscopic observation (scale bar = 50µ, magnification = 10×), **(C)** Percentage (%) of viable cells of crude methanolic extract (CME) from *A. sanguinolenta* and standards vincristine sulphate (VS) and 5-fluorouracil (5-FU) on HeLa cells **(D)** Percentage (%) of viable cells of petroleum ether fraction (PEF), Chloroform fraction (CHF), ethyl acetate fraction (EAF), and aqueous fraction (AQF) from *A. sanguinolenta* and standards vincristine sulphate (VS) and 5-fluorouracil (5-FU) on HeLa cells. The data is expressed as mean ± SD (n = 3) for all dosages tested. Values with *(*$p < 0.05$* and **$p < 0.01$*) were considered significant.

Assessment of Cytotoxicity of Chloroform Fraction (CHF) in Different Cancer Cell Lines

We again used the MTT assay to determine whether the CHF has cytotoxic activity on H-2228, H-3122, and HEK-293 cells. Surprisingly, CHF exerted a significant dose-dependent inhibition of H-2228 [**Fig. 7 (A)**], H-3122 [**Fig. 7 (B)**], and HEK-293 [**Fig. 7 (C)**] cell proliferation, suggesting that CHF has differential functions against other types of cancer.

Evaluation of *in vivo* Cytotoxicity

Given its superior *in vitro* antioxidant activity, the CHF fraction was selected for *in vivo* cytotoxic evaluation, with bleomycin as the reference standard. CHF administered intraperitoneally at 10.0 and 5.0 mg/kg

Journal of Chemical Health Risks
www.jchr.org
JCHR (2026) 16(2), 1292-1316 | ISSN:2251-6727

resulted in tumor growth inhibition of 77.2% and 52.0%, respectively, compared to untreated EAC controls (**Fig. 8**). Bleomycin achieved 87.48% inhibition. These findings suggest that CHF exhibits substantial anticancer potential, comparable to that of bleomycin, and may serve as a promising source of chemopreventive agents.

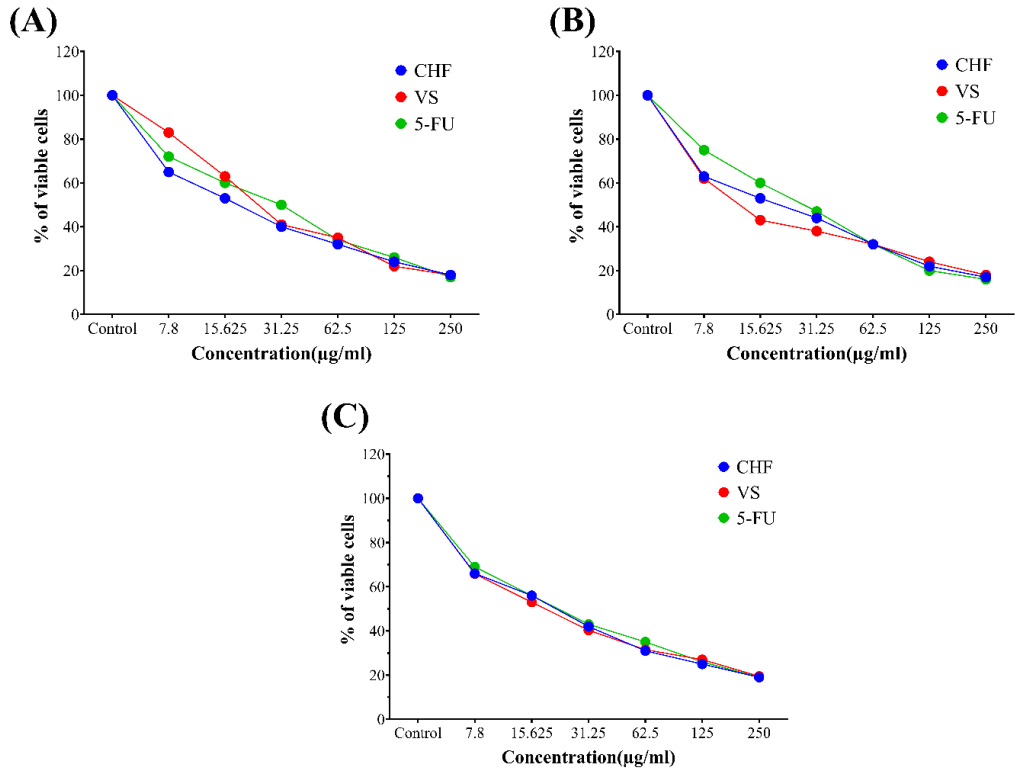

Fig. 7: % Growth inhibition of chloroform fraction (CHF) of *Aerva sanguinolenta* against **(A)** H-2228 **(B)** H-3122 **(C)** HEK-293 by the MTT assay

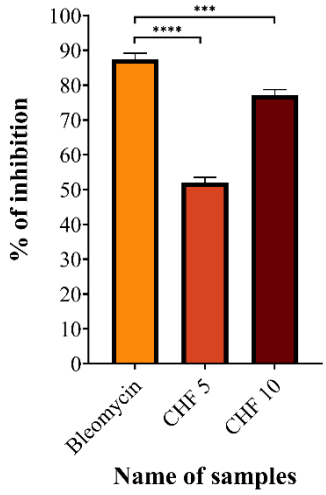

Fig. 8. Comparison of cell growth inhibition between the standard group and treatment groups.

Molecular Docking

Docking studies were conducted using the crystal structure of the p53 protein (PDB ID: 1YCQ). Binding energies for all compounds are presented in **Table 2**. Non-covalent interactions between 1YCQ and the 17 selected compounds, as well as the 1YCQ–Eprenetapopt complex, are depicted in **Fig. 9** and **Table 2**.

ADME Properties of Compounds

Physicochemical and ADME profiles of the compounds are summarized in **Tables 3** and **4**, supporting their potential suitability for drug development. Additional pharmacokinetic predictions were generated using the pkCSM server.

Journal of Chemical Health Risks
www.jchr.org
JCHR (2026) 16(2), 1292-1316 | ISSN:2251-6727

Table 2: Binding affinity scores of *A. sanguinolenta* identified molecules.

Name of Compounds	Chemical Class	Chemical Structure	Binding Score
2(4H)-Benzofuranone, 5,6,7,7a-tetrahydro-4,4,7a-trimethyl-, (R)-	Benzofuran derivative	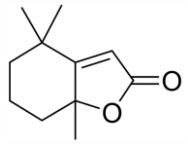	-5.2
9,12-Octadecadienoic acid, methyl ester	Methyl ester of polyunsaturated fatty acid	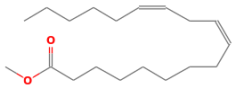	-4.8
9-Octadecenoic acid, methyl ester, (E)-	Methyl ester of monounsaturated fatty acid	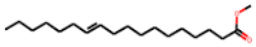	-4.6
3,7,11,15-Tetramethyl-2-hexadecen-1-ol	Terpenoid alcohol	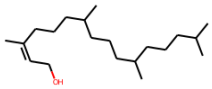	-4.6
2-Methoxy-4-vinylphenol	Phenolic compound	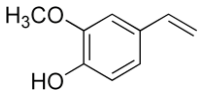	-4.4
9-Hexadecenoic acid, methyl ester, (Z)-	Methyl ester of fatty acid	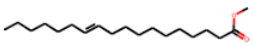	-4.4
11-Octadecenoic acid, methyl ester	Methyl ester of monounsaturated fatty acid	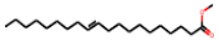	-4.4
Benzeneacetaldehyde	Aromatic aldehyde	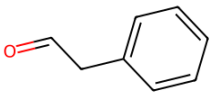	-4.3
7-Hexadecenoic acid, methyl ester, (Z)-	Methyl ester of fatty acid	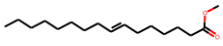	-4.3

Journal of Chemical Health Risks
www.jchr.org
JCHR (2026) 16(2), 1292-1316 | ISSN:2251-6727

Hexadecanoic acid, methyl ester	Methyl ester of fatty acid	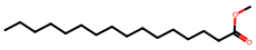	-4.3
Methyl stearate	Methyl ester of saturated fatty acid	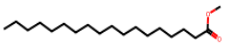	-4.3
1H-Pyrrole-2,5-dione, 3-ethyl-4-methyl-	Pyrrole derivative	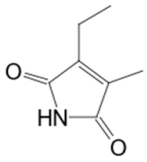	-4.2
Eprenetapopt	Quinuclidines	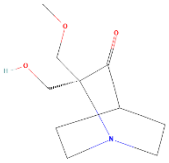	-4.2

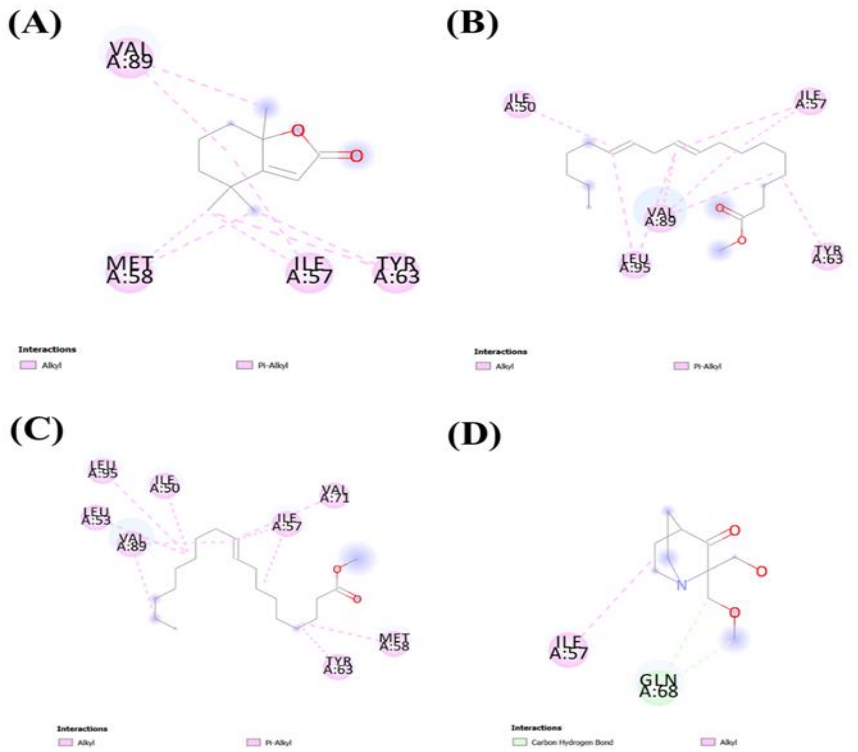

Fig. 9. 2D representation of top 3 docking scores **(A)** 2(4H)-Benzofuranone, 5,6,7,7a-tetrahydro- 4,4,7a-trimethyl-, (R)- **(B)** 9,12-Octadecadienoic acid, methyl ester **(C)** 9-Octadecenoic acid, methyl ester, (E)- and **(D)** Eprenetapopt (reference drug)

Journal of Chemical Health Risks
www.jchr.org
JCHR (2026) 16(2), 1292-1316 | ISSN:2251-6727

Table 3: Molecular properties of selected molecules and reference drug.

Ligand Name	Molecular weight g/mol	Num. H-bond acceptors	Num. H-bond donors	Fraction Csp3	TPSA (Å²)	Log Po/w	Log S (ESOL)	Lipinski Rule	Bioavailability Score
2(4H)-Benzofuranone, 5,6,7,7a-tetrahydro-4,4,7a-trimethyl-, (R)-	180.24	2	0	0.73	26.30	2.29	-2.32	Yes; 0 violation	0.55
9,12-Octadecadienoic acid, methyl ester	294.47	2	0	0.74	26.30	-	-	-	-
9-Octadecenoic acid, methyl ester, (E)-	296.49	2	0	0.84	26.30	4.75	-5.32	Yes; 1 violation	0.55
3,7,11,15-Tetramethyl-2-hexadecen-1-ol	296.53	1	1	0.90	20.23	4.66	-5.98	Yes; 1 violation	0.55
2-Methoxy-4-vinylphenol	150.17	2	1	0.11	29.46	2.14	-2.81	Yes; 0 violation	0.55
9-Hexadecenoic acid, methyl ester, (Z)-	268.43	2	0	0.82	26.30	4.44	-4.59	Yes; 1 violation	0.55
11-Octadecenoic acid, methyl ester	296.49	2	0	0.84	26.30	4.79	-5.32	Yes; 1 violation	0.55
Benzeneacetaldehyde	120.15	1	0	0.12	17.07	1.33	-2.07	Yes; 0 violation	0.55
7-Hexadecenoic acid, methyl ester, (Z)-	268.43	2	0	0.82	26.30	4.32	-4.59	Yes; 1 violation	0.55
Hexadecanoic acid, methyl ester	270.45	2	0	0.94	26.30	4.41	-5.18	Yes; 1 violation	0.55
Methyl stearate	298.50	2	0	0.95	26.30	4.81	-5.83	Yes; 1 violation	0.55
1H-Pyrrole-2,5-dione, 3-ethyl-4-methyl-	139.15	2	1	0.43	46.17	1.28	-0.94	Yes; 0 violation	0.55
Eprenetapopt	199.25	4	1	0.90	49.77	2.02	-0.82	Yes; 0 violation	0.55

Journal of Chemical Health Risks
www.jchr.org
JCHR (2026) 16(2), 1292-1316 | ISSN:2251-6727

Table 4: ADMET study of selected molecules and reference drug.

Ligand No.	Absorption		Distribution		Metabolism		Excretion		Toxicity	
	Water Solubility (log mol/L)	Human Intestinal absorption (%)	BBB permeability (log BB)	CNS Permeability (log PS)	CYP3A4 substrate	CYP3A4 inhibitor	Total Clearance (log ml/min/kg)	Renal OCT2 substrate	Human Max. tolerated dose (log mg/kg/day)	Oral Rat Acute Toxicity, LD50 (mol/kg)
2(4H)-Benzofuranone, 5,6,7,7a-tetrahydro-4,4,7a-trimethyl-, (R)-	-2.391	96.796	0.286	-2.802	No	No	1.051	No	0.575	1.987
9,12-Octadecadienoic acid, methyl ester	-7.343	92.66	0.767	-1.463	Yes	No	2.032	No	-0.019	1.617
9-Octadecenoic acid, methyl ester, (E)-	-7.436	92.154	0.777	-1.516	Yes	No	1.981	No	0.04	1.637
3,7,11,15-Tetramethyl-2-hexadecen-1-ol	-7.554	90.71	0.806	-1.563	Yes	No	1.686	No	0.05	1.607
2-Methoxy-4-vinylphenol	-1.958	91.965	0.289	-2.042	No	No	0.233	No	1.067	2.076
9-Hexadecenoic acid, methyl ester, (Z)-	-6.806	92.841	0.739	-1.625	Yes	No	1.914	No	0.125	1.608
11-Octadecenoic acid, methyl ester	-7.436	92.154	0.777	-1.516	Yes	No	1.98	No	0.04	1.637
Benzeneacetaldehyde	-1.508	95.899	0.158	-1.684	No	No		No	0.892	1.695

Journal of Chemical Health Risks
www.jchr.org
JCHR (2026) 16(2), 1292-1316 | ISSN:2251-6727

							0.331			
7-Hexadecenoic acid, methyl ester, (Z)-	-6.806	92.841	0.739	-1.625	Yes	No	1.915	No	0.125	1.608
Hexadecanoic acid, methyl ester	-6.927	92.335	0.749	-1.678	Yes	No	1.861	No	0.178	1.635
Methyl stearate	-7.51	91.648	0.787	0.787	Yes	No	1.929	No	0.099	1.656
1H-Pyrrole-2,5-dione, 3-ethyl-4-methyl-	-0.709	91.348	-0.223	-2.616	No	No	0.261	No	0.977	1.932
Eprenetapopt	-0.952	83.747	-0.193	-3.1	No	No	1.153	No	0.148	1.978

Toxicity Predictions

Toxicity assessment revealed that none of the 17 compounds exhibited hepatotoxicity, cytotoxicity, immunotoxicity, or mutagenicity, except 2-methoxy-4-vinylphenol (immunotoxicity) and benzeneacetaldehyde (carcinogenicity) (**Table 5**). Overall, the compounds demonstrated favourable safety profiles and good oral bioavailability, underscoring their potential as lead candidates for further drug development.

Table 5: Toxicity prediction compounds with reference drug.

Ligand name	Hepatotoxicity	Carcinogenicity	Immunotoxicity	Mutagenicity	Cytotoxicity
2(4H)-Benzofuranone, 5,6,7,7a-tetrahydro-4,4,7a-trimethyl-, (R)-	Inactive	Inactive	Inactive	Inactive	Inactive

Journal of Chemical Health Risks
www.jchr.org
JCHR (2026) 16(2), 1292-1316 | ISSN:2251-6727

9,12-Octadecadienoic acid, methyl ester	Inactive	Inactive	Inactive	Inactive	Inactive
9-Octadecenoic acid, methyl ester, (E)-	Inactive	Inactive	Inactive	Inactive	Inactive
3,7,11,15-Tetramethyl-2-hexadecen-1-ol	Inactive	Inactive	Inactive	Inactive	Inactive
2-Methoxy-4-vinylphenol	Inactive	Inactive	Active	Inactive	Inactive
9-Hexadecenoic acid, methyl ester, (Z)-	Inactive	Inactive	Inactive	Inactive	Inactive
11-Octadecenoic acid, methyl ester	Inactive	Inactive	Inactive	Inactive	Inactive
Benzeneacetaldehyde	Inactive	Active	Inactive	Inactive	Inactive
7-Hexadecenoic acid, methyl ester, (Z)-	Inactive	Inactive	Inactive	Inactive	Inactive
Hexadecanoic acid, methyl ester	Inactive	Inactive	Inactive	Inactive	Inactive
Methyl stearate	Inactive	Inactive	Inactive	Inactive	Inactive
1H-Pyrrole-2,5-dione, 3-ethyl-4-methyl-	Inactive	Inactive	Inactive	Inactive	Inactive
Eprenetapopt	Inactive	Inactive	Inactive	Inactive	Inactive

Discussion

The increasing interest in plant-based therapeutics has led to extensive research on phytoconstituents with antioxidant and anticancer potential. In this study, *A. sanguinolenta* exhibited significant antioxidant activity, largely attributable to its rich phenolic and flavonoid content, particularly in the chloroform fraction (CHF). These phytochemicals are well-documented redox modulators capable of neutralizing reactive oxygen species (ROS), thereby mitigating oxidative stress, a known contributor to carcinogenesis [31].

Multiple antioxidant assays confirmed the concentration-dependent activity of all extracts, with CHF consistently demonstrating the highest efficacy. Its superior performance in phosphomolybdenum and ferric-reducing power assays underscores the relevance of its phenolic content. These findings align with earlier reports that link phenolics and flavonoids to strong electron- or hydrogen-donating capacity and free radical scavenging mechanisms [32, 33].

DPPH and hydroxyl radical assays further validated the antioxidant potential of CHF, which approached the activity of standard antioxidants, such as BHT [34, 35]. Given the high reactivity of hydroxyl radicals in initiating lipid peroxidation and DNA damage [36], CHF's efficacy in scavenging these radicals suggests its potential role in cancer prevention. In agreement, the lipid peroxidation assay revealed that CHF had the lowest IC_{50} value (22.4 µg/mL), indicating strong membrane-protective effects [37, 38].

Cytotoxicity studies using both the brine shrimp lethality bioassay and MTT cell proliferation assay strongly substantiated the antiproliferative efficacy of *A. sanguinolenta* extracts, particularly CHF. Among all tested fractions, CME, CHF, and EAF exhibited marked cytotoxicity against HeLa cervical cancer cells, with IC_{50} values (17–21 µg/mL) comparable to standard drugs [38]. The morphological alterations observed under microscopy, cell shrinkage, nuclear condensation, and detachment from the culture surface suggest that the mechanism of cell death is primarily apoptotic rather than necrotic. This is consistent with the known ability of phenolic compounds to induce mitochondrial membrane depolarization, activate caspase cascades, and promote DNA fragmentation in malignant cells. These findings confirm that the bioactive constituents of *A. sanguinolenta* exert potent inhibitory effects on cancer cell proliferation at relatively low concentrations. Notably, CHF demonstrated the strongest cytotoxic response, suggesting that its rich composition of polyphenolic and aromatic compounds is responsible for

Journal of Chemical Health Risks
www.jchr.org
JCHR (2026) 16(2), 1292-1316 | ISSN:2251-6727

enhanced biological activity. Beyond its activity against HeLa cells, CHF also showed significant dose-dependent inhibition of H-2228, H-3122, and HEK-293 cell proliferation, indicating a broad-spectrum anticancer profile that extends across epithelial and lung cancer lineages. The inhibition observed in these lines highlights the possible multi-target nature of CHF phytoconstituents, which may interact with diverse molecular pathways involved in tumor growth and survival. These effects are likely mediated by polyphenolic-induced apoptosis and DNA damage. Structure–activity relationship (SAR) analysis suggests that small, polar molecules with aromatic or heterocyclic moieties, characteristics dominant in CHF, may account for the stronger bioactivity observed.

In vivo evaluation demonstrated that CHF achieved 77.2% tumor growth inhibition at a relatively low dose of 10 mg/kg, underscoring *A. sanguinolenta* as a promising source of natural antioxidants with pronounced antitumor potential. EAC cells, widely employed in antiproliferative research, have been shown in numerous studies to be susceptible to plant-derived cytotoxic agents [36]. In the present work, cell counts confirmed that *A. sanguinolenta* significantly ($p < 0.001$) suppressed tumor cell proliferation, with efficacy approaching that of bleomycin. Mechanistically, cancer cells often exhibit elevated ROS levels that activate proliferative and survival pathways such as PI3K/AKT, MAPK, and NF-κB. The potent antioxidants present in CHF may attenuate these pathways by reducing ROS accumulation, thereby inducing apoptosis or growth arrest. Furthermore, the p53 protein, a central regulator of apoptosis, DNA repair, and cell cycle control, represents a critical target for anticancer drug development, and the *in silico* findings herein support its potential modulation by CHF-derived compounds [37].

In this study, 17 compounds targeting the p53 protein were analyzed for potential efficacy against EAC cancer. Molecular docking was employed to identify candidates with superior binding affinity [38, 39], and the top 12 compounds were shortlisted based on higher affinity compared to the synthetic reference drug (**Table 2**). Subsequent pharmacokinetic evaluations were performed, as optimization of these properties is critical for advancing compounds through clinical trials to viable drug candidates [40]. Molecular weight and topological polar surface area (TPSA) influence membrane permeability, with lower values generally enhancing absorption. Lipophilicity (LogP), the logarithmic ratio of solubility in organic to aqueous phases, significantly affects absorption; lower LogP values favor uptake. Solubility (LogS) is another key parameter, with lower values indicating better solubility [41]. Excess hydrogen bond donors or acceptors can hinder membrane permeability. ADMET predictions indicated that four compounds met acceptable ranges for potential drug candidacy. Given the intended action against brain disorders, blood–brain barrier (BBB) permeability was also considered essential [42]. Toxicity remains a leading cause of late-stage drug development failure [43]; thus, *in silico* toxicity analysis was performed to circumvent the limitations of *in vivo* methods, including ethical concerns, cost, and time. The analysis revealed that none of the top 12 compounds were carcinogenic.

The ADMET analysis revealed that all selected molecules exhibited excellent human intestinal absorption (90.71–96.80%) [44], moderate water solubility (log mol/L: –7.554 to –0.709), and variable blood–brain barrier permeability (0.158–0.806) [45]. Most were identified as CYP3A4 substrates, suggesting significant hepatic metabolism with minimal risk of CYP3A4-mediated drug–drug interactions [46]. Total clearance values (0.233–2.032 log ml/min/kg) indicated varying elimination rates, and none were substrates for renal OCT2, implying negligible involvement of this pathway [47]. The human maximum tolerated dose ranged from –0.019 to 1.067 log mg/kg/day, while oral rat acute toxicity (LD_{50}) values were 1.607–2.076 mol/kg, reflecting moderate toxicity. Overall, the compounds demonstrated favorable pharmacokinetic profiles, although further optimization of solubility and toxicity may be required for safe and effective therapeutic use.

Collectively, our results suggest that the antioxidant and anticancer activities of *A. sanguinolenta* are primarily driven by CHF, owing to its enriched content of redox-active phenolics and structurally favourable minor compounds. The integration of *in vitro*, *in vivo* proxy models, and *in silico* analyses offers a robust foundation for future preclinical evaluation of this plant as a source of potential anticancer agents.

Conclusion

Journal of Chemical Health Risks

www.jchr.org

JCHR (2026) 16(2), 1292-1316 | ISSN:2251-6727

This study demonstrates that *Aerva sanguinolenta* (L.) Blume, particularly its chloroform fraction (CHF), is a rich source of redox-active phytochemicals with notable anticancer potential. CHF exhibited the highest antioxidant activity, potent cytotoxicity against HeLa (cervical), H-2228 and H-3122 (lung), and HEK-293 (renal epithelial) cells, and significant *in vivo* tumor inhibition in Ehrlich ascites carcinoma–bearing mice (77.2% at 10 mg/kg). GC–MS analysis identified bioactive compounds with strong p53-binding affinities, and ADMET predictions indicated favourable pharmacokinetics and safety profiles, though solubility optimization may be required. These findings provide a strong foundation for further mechanistic studies and preclinical development of CHF-derived compounds as cost-effective plant-based anticancer agents.

Ethics Approval

All methods of animal experiments were implemented following proper rules and directives of the institution, along with ethical authorization granted from the Institute of Biological Sciences (IBSc), Rajshahi University, Bangladesh (license no: 72 (23)/320/IAMEBBC/IBSc).

Funding

We declare that we have a research grant (2048/5/52/R.U./Science-48/2023-24) from the Faculty of Science, University of Rajshahi, Bangladesh.

Authors' Contributions

Joy Sarker: Methodology, Formal analysis, Investigation, Validation, Software, Data Curation, Writing - Original Draft. **A.S.M. Ali Reza, A.B.M. Ashraful:** Software, Formal analysis, Data Curation, Writing - Original Draft. **Md. Sabbir Hossain, Aziz Abdur Rahman, Mamunur Rashid, Md. Golam Sadik:** Validation, Writing - Review & Editing. **Adeeba Anjum, Runa Akter, Md. Jasim Uddin:** Funding acquisition, Writing - Review & Editing. **AHM Khurshid Alam:** Conceptualization, Resources, Visualization, Supervision, Writing - Finalize Original Draft, Project Administration.

Acknowledgments

The authors wish to thank the Faculty of Science for providing a research grant (2048/5/52/R.U./Science-48/2023-24) and the Department of Pharmacy, University of Rajshahi, for their kind support in the progress of the research.

Disclosure Statement

We neither have any conflicts of interest regarding this publication nor substantial financial support that might have influenced the outcomes.

References

(1) Bray, F.; Laversanne, M.; Sung, H.; Ferlay, J.; Siegel, R. L.; Soerjomataram, I.; Jemal, A. Global cancer statistics 2022: GLOBOCAN estimates of incidence and mortality worldwide for 36 cancers in 185 countries. *CA: a cancer journal for clinicians* **2024**, *74* (3), 229-263.

(2) Hashem, S.; Ali, T. A.; Akhtar, S.; Nisar, S.; Sageena, G.; Ali, S.; Al-Mannai, S.; Therachiyil, L.; Mir, R.; Elfaki, I. Targeting cancer signaling pathways by natural products: Exploring promising anti-cancer agents. *Biomedicine & Pharmacotherapy* **2022**, *150*, 113054.

(3) Pramesh, C.; Badwe, R. A.; Bhoo-Pathy, N.; Booth, C. M.; Chinnaswamy, G.; Dare, A. J.; de Andrade, V. P.; Hunter, D. J.; Gopal, S.; Gospodarowicz, M. Priorities for cancer research in low-and middle-income countries: a global perspective. *Nature medicine* **2022**, *28* (4), 649-657.

(4) Iqbal, M. J.; Kabeer, A.; Abbas, Z.; Siddiqui, H. A.; Calina, D.; Sharifi-Rad, J.; Cho, W. C. Interplay of oxidative stress, cellular communication and signaling pathways in cancer. *Cell Communication and Signaling* **2024**, *22* (1), 7.

(5) Xian, D.; Lai, R.; Song, J.; Xiong, X.; Zhong, J. Emerging perspective: role of increased ROS and redox imbalance in skin carcinogenesis. *Oxidative medicine and cellular longevity* **2019**, *2019* (1), 8127362.

(6) Kozlov, A. V.; Javadov, S.; Sommer, N. Cellular ROS and antioxidants: physiological and pathological role. MDPI: 2024; Vol. 13, p 602.

(7) Gordaliza, M. Natural products as leads to anticancer drugs. *Clinical and Translational Oncology* **2007**, *9* (12), 767-776.

(8) Alamgir, A. Biotechnology, in vitro production of natural bioactive compounds, herbal preparation, and disease management (treatment and prevention). In *Therapeutic use of medicinal plants and their*

Journal of Chemical Health Risks

www.jchr.org

JCHR (2026) 16(2), 1292-1316 | ISSN:2251-6727

extracts: volume 2: phytochemistry and bioactive compounds, Springer, 2018; pp 585-664.

(9) İSTANBULLUGİL, F. R. Natural Products/Bioactive Compounds as a Source of Anticancer Drugs. **2023**.

(10) Sarker, J.; Ali, M. R.; Khan, M. A.; Rahman, M. M.; Hossain, A.; Alam, A. The plant aerva sanguinolenta: A review on traditional uses, phytoconstituents and pharmacological activities. *Pharmacognosy Reviews* **2019**, *13* (26), 89.

(11) Maqbool, M.; Muhammad, A.; Muhammad, I.; Waheeda, M.; Tanveer, H.; Waqas, A. Investigation of antimicrobial and antioxidant activity of Aerva sanguinolenta (l.) Blume from district Bhimber (AJK), Pakistan. *Bioscience Research* **2021**, *18* (1), 640-652.

(12) Hossain, F.; Zamaly, S.; Ashraful, A.; Rahman, A. A.; Sadik, G.; Khurshid Alam, A. Exploring the therapeutic potential of Leea rubra (Vitaceae): Antioxidant efficacy, brine shrimp lethality, and in vivo anticancer activity against EAC cells in Swiss albino mice. *Journal of Biologically Active Products from Nature* **2025**, *15* (2), 181-195.

(13) Sadeghi, M.; Khomartash, M. S.; Gorgani-Firuzjaee, S.; Vahidi, M.; Khiavi, F. M.; Taslimi, P. α-glucosidase inhibitory, antioxidant activity, and GC/MS analysis of Descurainia sophia methanolic extract: In vitro, in vivo, and in silico studies. *Arabian journal of chemistry* **2022**, *15* (9), 104055.

(14) Mostofa, M. G.; Reza, A. A.; Khan, Z.; Munira, M. S.; Khatoon, M. M.; Kabir, S. R.; Sadik, M. G.; Ağagündüz, D.; Capasso, R.; Kazi, M. Apoptosis-inducing anti-proliferative and quantitative phytochemical profiling with in silico study of antioxidant-rich Leea aequata L. leaves. *Heliyon* **2024**, *10* (1).

(15) Reza, A. A.; Nasrin, M. S.; Alam, A. K. Phytochemicals, Antioxidants, and Cholinesterase Inhibitory Profiles of Elatostema Papillosum Leaves: An Alternative Approach for Management of Alzheimer's Disease. **2018**.

(16) Prieto, P.; Pineda, M.; Aguilar, M. Spectrophotometric quantitation of antioxidant capacity through the formation of a phosphomolybdenum complex: specific application to the determination of vitamin E. *Analytical biochemistry* **1999**, *269* (2), 337-341.

(17) Oyaizu, M. Studies on products of browning reaction. Antioxidant activities of products of browning reaction prepared from glucoamine. *Jap. J. Nutri 986* (44), 307-315.

(18) Blois, M. S. Antioxidant determinations by the use of a stable free radical. *nature* **1958**, *181* (4617), 1199-1200.

(19) Halliwell, B. Lipid peroxidation: a radical chain reaction. *Free radicals in biology and medicine* **1989**.

(20) Haenen, G. R.; Bast, A. Protection against lipid peroxidation by a microsomal glutathione-dependent labile factor. *FEBS letters* **1983**, *159* (1-2), 24-28.

(21) Abeyrathne, E. D. N. S.; Nam, K.; Ahn, D. U. Analytical methods for lipid oxidation and antioxidant capacity in food systems. *Antioxidants* **2021**, *10* (10), 1587.

(22) Meyer, B.; Ferrigni, N.; Putnam, J.; Jacobsen, L.; Nichols, D.; McLaughlin, J. L. Brine shrimp: a convenient general bioassay for active plant constituents. *Planta medica* **1982**, *45* (05), 31-34.

(23) Islam, S.; Nasrin, S.; Khan, M. A.; Hossain, A. S.; Islam, F.; Khandokhar, P.; Mollah, M. N. H.; Rashid, M.; Sadik, G.; Rahman, M. A. A. Evaluation of antioxidant and anticancer properties of the seed extracts of Syzygium fruticosum Roxb. growing in Rajshahi, Bangladesh. *BMC complementary and alternative medicine* **2013**, *13* (1), 142.

(24) Rahman, M. M.; Reza, A. M. A.; Khan, M. A.; Sujon, K. M.; Sharmin, R.; Rashid, M.; Sadik, M. G.; Reza, M. A.; Tsukahara, T.; Capasso, R. Unfolding the Apoptotic Mechanism of Antioxidant Enriched-Leaves of Tabebuia pallida (Lindl.) Miers in EAC Cells and Mouse Model. *Journal of Ethnopharmacology* **2021**, 114297.

(25) Hossain, M. S.; Ashraful, A.; Rahman, A. A.; Rashid, M.; Sadik, M. G.; Khurshid Alam, A. Anti-ROS and Anticancer Potential of Rhizomes and a Polyunsaturated Fatty Acid From Chloroform Fraction of Curcuma wallichii as a Bioactive Compound. *Journal of Food Biochemistry* **2025**, *2025* (1), 9517484.

(26) Nag, A.; Paul, S.; Banerjee, R.; Kundu, R. In silico study of some selective phytochemicals against a hypothetical SARS-CoV-2 spike RBD using

Journal of Chemical Health Risks
www.jchr.org
JCHR (2026) 16(2), 1292-1316 | ISSN:2251-6727

molecular docking tools. *Computers in Biology and Medicine* **2021**, *137*, 104818.
(27) Kondapuram, S. K.; Sarvagalla, S.; Coumar, M. S. Docking-based virtual screening using PyRx Tool: autophagy target Vps34 as a case study. In *Molecular docking for computer-aided drug design*, Elsevier, 2021; pp 463-477.
(28) Singh, A.; Vellapandian, C. In silico and pharmacokinetic assessment of echinocystic acid effectiveness in Alzheimer's disease like pathology. *Future Science OA* **2024**, *10* (1), FSO904.
(29) De Carlo, A.; Ronchi, D.; Piastra, M.; Tosca, E. M.; Magni, P. Predicting admet properties from molecule smile: a bottom-up approach using attention-based graph neural networks. *Pharmaceutics* **2024**, *16* (6), 776.
(30) Banerjee, P.; Eckert, A. O.; Schrey, A. K.; Preissner, R. ProTox-II: a webserver for the prediction of toxicity of chemicals. *Nucleic acids research* **2018**, *46* (W1), W257-W263.
(31) Khan, M. A.; Rahman, M. M.; Sardar, M. N.; Arman, M. S. I.; Islam, M. B.; Khandakar, M. J. A.; Rashid, M.; Sadik, G.; Alam, A. K. Comparative investigation of the free radical scavenging potential and anticancer property of Diospyros blancoi (Ebenaceae). *Asian Pacific Journal of Tropical Biomedicine* **2016**, *6* (5), 410-417.
(32) Oliveira, I.; Sousa, A.; Ferreira, I. C.; Bento, A.; Estevinho, L.; Pereira, J. A. Total phenols, antioxidant potential and antimicrobial activity of walnut (Juglans regia L.) green husks. *Food and chemical toxicology* **2008**, *46* (7), 2326-2331.
(33) Sabourin-Provost, G.; Hallenbeck, P. C. High yield conversion of a crude glycerol fraction from biodiesel production to hydrogen by photofermentation. *Bioresource technology* **2009**, *100* (14), 3513-3517.
(34) Reddy, B. S.; Reddy, R. K. K.; Reddy, B. P.; Ramakrishna, S.; Diwan, P. V. Potential in vitro antioxidant and protective effects of Soymida febrifuga on ethanol induced oxidative damage in HepG2 cells. *Food and chemical toxicology* **2008**, *46* (11), 3429-3442.
(35) Duan, X.; Wu, G.; Jiang, Y. Evaluation of the antioxidant properties of litchi fruit phenolics in relation to pericarp browning prevention. *Molecules* **2007**, *12* (4), 759-771.
(36) Pandey, A.; Mishra, A.; Mishra, A. Antifungal and antioxidative potential of oil and extracts derived from leaves of Indian spice plant Cinnamomum tamala. *Cellular and Molecular Biology* **2012**, *58* (1), 142-147.
(37) Ali Reza, A.; Hossain, M. S.; Akhter, S.; Rahman, M. R.; Nasrin, M. S.; Uddin, M. J.; Sadik, G.; Khurshid Alam, A. In vitro antioxidant and cholinesterase inhibitory activities of Elatostema papillosum leaves and correlation with their phytochemical profiles: a study relevant to the treatment of Alzheimer's disease. *BMC complementary and alternative medicine* **2018**, *18* (1), 123.
(38) Khan, M. A.; Rahman, A. A.; Islam, S.; Khandokhar, P.; Parvin, S.; Islam, M. B.; Hossain, M.; Rashid, M.; Sadik, G.; Nasrin, S. A comparative study on the antioxidant activity of methanolic extracts from different parts of Morus alba L.(Moraceae). *BMC Research Notes* **2013**, *6* (1), 24.
(39) Shah, H. D.; Saranath, D.; Murthy, V. A molecular dynamics and docking study to screen anti-cancer compounds targeting mutated p53. *J Biomol Struct Dyn* **2022**, *40* (6), 2407-2416. DOI: 10.1080/07391102.2020.1839559 From NLM.
(40) Lazerwith, S. E.; Bahador, G.; Canales, E.; Cheng, G.; Chong, L.; Clarke, M. O.; Doerffler, E.; Eisenberg, E. J.; Hayes, J.; Lu, B.; et al. Optimization of Pharmacokinetics through Manipulation of Physicochemical Properties in a Series of HCV Inhibitors. *ACS Med Chem Lett* **2011**, *2* (10), 715-719. DOI: 10.1021/ml200163b From NLM.
(41) Cornelissen, F. M. G.; Markert, G.; Deutsch, G.; Antonara, M.; Faaij, N.; Bartelink, I.; Noske, D.; Vandertop, W. P.; Bender, A.; Westerman, B. A. Explaining Blood-Brain Barrier Permeability of Small Molecules by Integrated Analysis of Different Transport Mechanisms. *J Med Chem* **2023**, *66* (11), 7253-7267. DOI: 10.1021/acs.jmedchem.2c01824 From NLM.
(42) Russell, S. Meta-models for predicting blood brain barrier penetration based on simple physicochemical descriptors. Google Patents: 2003.
(43) Hwang, T. J.; Carpenter, D.; Lauffenburger, J. C.; Wang, B.; Franklin, J. M.; Kesselheim, A. S. Failure of investigational drugs in late-stage clinical

development and publication of trial results. *JAMA internal medicine* **2016**, *176* (12), 1826-1833.

(44) Guan, L.; Yang, H.; Cai, Y.; Sun, L.; Di, P.; Li, W.; Liu, G.; Tang, Y. ADMET-score - a comprehensive scoring function for evaluation of chemical drug-likeness. *Medchemcomm* **2019**, *10* (1), 148-157. DOI: 10.1039/c8md00472b From NLM.

(45) Bergström, C. A. S.; Larsson, P. Computational prediction of drug solubility in water-based systems: Qualitative and quantitative approaches used in the current drug discovery and development setting. *Int J Pharm* **2018**, *540* (1-2), 185-193. DOI: 10.1016/j.ijpharm.2018.01.044 From NLM.

(46) Kenworthy, K. E.; Bloomer, J. C.; Clarke, S. E.; Houston, J. B. CYP3A4 drug interactions: correlation of 10 in vitro probe substrates. *Br J Clin Pharmacol* **1999**, *48* (5), 716-727. DOI: 10.1046/j.1365-2125.1999.00073.x From NLM.

(47) Motohashi, H.; Inui, K. Organic cation transporter OCTs (SLC22) and MATEs (SLC47) in the human kidney. *Aaps j* **2013**, *15* (2), 581-588. DOI: 10.1208/s12248-013-9465-7 From NLM.